Two-dimensional analysis of Bose-Einstein correlations in hadronic Z decays at LEP

The ALEPH Collaboration

A. Heister, S. Schael
Physikalisches Institut das RWTH-Aachen, 52056 Aachen, Germany

R. Barate, R. Brunelière, I. De Bonis, D. Decamp, C. Goy, S. Jézéquel, J.-P. Lees, F. Martin, E. Merle, M.-N. Minard, B. Pietrzyk, B. Trocmé
Laboratoire de Physique des Particules (LAPP), IN[2]P[3]-CNRS, 74019 Annecy-le-Vieux Cedex, France

S. Bravo, M.P. Casado, M. Chmeissani, J.M. Crespo, E. Fernandez, M. Fernandez-Bosman, Ll. Garrido,[15] M. Martinez, A. Pacheco, H. Ruiz
Institut de Física d'Altes Energies, Universitat Autònoma de Barcelona, 08193 Bellaterra (Barcelona), Spain[7]

A. Colaleo, D. Creanza, N. De Filippis, M. de Palma, G. Iaselli, G. Maggi, M. Maggi, S. Nuzzo, A. Ranieri, G. Raso,[24] F. Ruggieri, G. Selvaggi, L. Silvestris, P. Tempesta, A. Tricomi,[3] G. Zito
Dipartimento di Fisica, INFN Sezione di Bari, 70126 Bari, Italy

X. Huang, J. Lin, Q. Ouyang, T. Wang, Y. Xie, R. Xu, S. Xue, J. Zhang, L. Zhang, W. Zhao
Institute of High Energy Physics, Academia Sinica, Beijing, P.R. China[8]

D. Abbaneo, T. Barklow,[26] O. Buchmüller,[26] M. Cattaneo, B. Clerbaux,[23] H. Drevermann, R.W. Forty, M. Frank, F. Gianotti, J.B. Hansen, J. Harvey, D.E. Hutchcroft,[30] P. Janot, B. Jost, M. Kado,[2] P. Mato, A. Moutoussi, F. Ranjard, L. Rolandi, D. Schlatter, G. Sguazzoni, F. Teubert, A. Valassi, I. Videau
European Laboratory for Particle Physics (CERN), 1211 Geneva 23, Switzerland

F. Badaud, S. Dessagne, A. Falvard,[20] D. Fayolle, P. Gay, J. Jousset, B. Michel, S. Monteil, D. Pallin, J.M. Pascolo, P. Perret
Laboratoire de Physique Corpusculaire, Université Blaise Pascal, IN[2]P[3]-CNRS, Clermont-Ferrand, 63177 Aubière, France

J.D. Hansen, J.R. Hansen, P.H. Hansen, A.C. Kraan, R. Muresan, B.S. Nilsson
Niels Bohr Institute, 2100 Copenhagen, DK-Denmark[9]

A. Kyriakis, C. Markou, E. Simopoulou, A. Vayaki, K. Zachariadou
Nuclear Research Center Demokritos (NRCD), 15310 Attiki, Greece

A. Blondel,[12] J.-C. Brient, F. Machefert, A. Rougé, H. Videau
Laoratoire Leprince-Ringuet, Ecole Polytechnique, IN[2]P[3]-CNRS, 91128 Palaiseau Cedex, France

V. Ciulli, E. Focardi, G. Parrini
Dipartimento di Fisica, Università di Firenze, INFN Sezione di Firenze, 50125 Firenze, Italy

A. Antonelli, M. Antonelli, G. Bencivenni, F. Bossi, G. Capon, F. Cerutti, V. Chiarella, P. Laurelli, G. Mannocchi,[5] G.P. Murtas, L. Passalacqua
Laboratori Nazionali dell'INFN (LNF-INFN), 00044 Frascati, Italy

J. Kennedy, J.G. Lynch, P. Negus, V. O'Shea, A.S. Thompson
Department of Physics and Astronomy, University of Glasgow, Glasgow G12 8QQ,United Kingdom[10]

S. Wasserbaech
Utah Valley State College, Orem, UT 84058, USA

R. Cavanaugh,[4] S. Dhamotharan,[21] C. Geweniger, P. Hanke, V. Hepp, E.E. Kluge, A. Putzer, H. Stenzel, K. Tittel, M. Wunsch[19]
Kirchhoff-Institut für Physik, Universität Heidelberg, 69120 Heidelberg, Germany[16]

R. Beuselinck, W. Cameron, G. Davies, P.J. Dornan, M. Girone,[1] R.D. Hill, N. Marinelli, J. Nowell, S.A. Rutherford,
J.K. Sedgbeer, J.C. Thompson,[14] R. White
Department of Physics, Imperial College, London SW7 2BZ, United Kingdom[10]

V.M. Ghete, P. Girtler, E. Kneringer, D. Kuhn, G. Rudolph
Institut für Experimentalphysik, Universität Innsbruck, 6020 Innsbruck, Austria[18]

E. Bouhova-Thacker, C.K. Bowdery, D.P. Clarke, G. Ellis, A.J. Finch, F. Foster, G. Hughes, R.W.L. Jones,
M.R. Pearson, N.A. Robertson, M. Smizanska
Department of Physics, University of Lancaster, Lancaster LA1 4YB, United Kingdom[10]

O. van der Aa, C. Delaere,[28] G.Leibenguth,[31] V. Lemaitre[29]
Institut de Physique Nucléaire, Département de Physique, Université Catholique de Louvain, 1348 Louvain-la-Neuve, Belgium

U. Blumenschein, F. Hölldorfer, K. Jakobs, F. Kayser, K. Kleinknecht, A.-S. Müller, B. Renk, H.-G. Sander,
S. Schmeling, H. Wachsmuth, C. Zeitnitz, T. Ziegler
Institut für Physik, Universität Mainz, 55099 Mainz, Germany[16]

A. Bonissent, P. Coyle, C. Curtil, A. Ealet, D. Fouchez, P. Payre, A. Tilquin
Centre de Physique des Particules de Marseille, Univ Méditerranée, IN^{2}P^3-CNRS, 13288 Marseille, France

F. Ragusa
Dipartimento di Fisica, Università di Milano e INFN Sezione di Milano, 20133 Milano, Italy

A. David, H. Dietl,[32] G. Ganis,[27] K. Hüttmann, G. Lütjens, W. Männer[32], H.-G. Moser, R. Settles, M. Villegas,
G. Wolf
Max-Planck-Institut für Physik, Werner-Heisenberg-Institut, 80805 München, Germany[P]

J. Boucrot, O. Callot, M. Davier, L. Duflot, J.-F. Grivaz, Ph. Heusse, A. Jacholkowska,[6] L. Serin, J.-J. Veillet
Laboratoire de l'Accélérateur Linéaire, Université de Paris-Sud, IN^{2}P^3-CNRS, 91898 Orsay Cedex, France

P. Azzurri, G. Bagliesi, T. Boccali, L. Foà, A. Giammanco, A. Giassi, F. Ligabue, A. Messineo, F. Palla, G. Sanguinetti,
A. Sciabà, P. Spagnolo, R. Tenchini, A. Venturi, P.G. Verdini
Dipartimento di Fisica dell'Università, INFN Sezione di Pisa, e Scuola Normale Superiore, 56010 Pisa, Italy

O. Awunor, G.A. Blair, G. Cowan, A. Garcia-Bellido, M.G. Green, T. Medcalf, A. Misiejuk, J.A. Strong,
P. Teixeira-Dias
Department of Physics, Royal Holloway & Bedford New College, University of London, Egham, Surrey TW20 OEX, United
Kingdom[10]

R.W. Clifft, T.R. Edgecock, P.R. Norton, I.R. Tomalin, J.J. Ward
Particle Physics Dept., Rutherford Appleton Laboratory, Chilton, Didcot, Oxon OX11 OQX, United Kingdom[10]

B. Bloch-Devaux, D. Boumediene, P. Colas, B. Fabbro, E. Lançon, M.-C. Lemaire, E. Locci, P. Perez, J. Rander,
B. Tuchming, B. Vallage
CEA, DAPNIA/Service de Physique des Particules, CE-Saclay, 91191 Gif-sur-Yvette Cedex, France[17]

A.M. Litke, G. Taylor
Institute for Particle Physics, University of California at Santa Cruz, Santa Cruz, CA 95064, USA[22]

C.N. Booth, S. Cartwright, F. Combley,[25] P.N. Hodgson, M. Lehto, L.F. Thompson
Department of Physics, University of Sheffield, Sheffield S3 7RH, United Kingdom[10]

A. Böhrer, S. Brandt, C. Grupen, J. Hess, A. Ngac, G. Prange
Fachbereich Physik, Universität Siegen, 57068 Siegen, Germany[16]

C. Borean, G. Giannini
Dipartimento di Fisica, Università di Trieste e INFN Sezione di Trieste, 34127 Trieste, Italy

H. He, J. Putz, J. Rothberg
Experimental Elementary Particle Physics, University of Washington, Seattle, WA 98195 USA

S.R. Armstrong, K. Berkelman, K. Cranmer, D.P.S. Ferguson, Y. Gao,[13] S. González, O.J. Hayes, H. Hu, S. Jin, J. Kile,
P.A. McNamara III, J. Nielsen, Y.B. Pan, J.H. von Wimmersperg-Toeller, W. Wiedenmann, J. Wu, Sau Lan Wu,
X. Wu, G. Zobernig
Department of Physics, University of Wisconsin, Madison, WI 53706, USA[11]

I. Aracena[33], G. Dissertori
Institute for Particle Physics, ETH Hönggerberg, 8093 Zürich, Switzerland

Abstract. Bose-Einstein correlations are studied in pairs of charged pions from hadronic Z decays, collected by the ALEPH detector. The correlation function, measured using either the unlike-sign or the mixed reference sample, is studied in terms of the Lorentz-invariant four-momentum difference and its transverse, Q_{T}, and longitudinal, Q_{L}, components with respect to the longitudinal centre-of-mass system. Values for the correlation radii, R_{T} and R_{L}, are obtained from the fit of the Goldhaber parametrisation. The results indicate that the correlation radii values depend on the chosen kind of reference sample and on the two-jet purity.

[1] Also at CERN, 1211 Geneva 23, Switzerland.

[2] Now at Fermilab, PO Box 500, MS 352, Batavia, IL 60510, USA.

[3] Also at Dipartimento di Fisica di Catania and INFN Sezione di Catania, 95129 Catania, Italy.

[4] Now at University of Florida, Department of Physics, Gainesville, Florida 32611-8440, USA.

[5] Also Istituto di Cosmo-Geofisica del C.N.R., Torino, Italy.

[6] Also at Groupe d'Astroparticules de Montpellier, Université de Montpellier II, 34095, Montpellier, France.

[7] Supported by CICYT, Spain.

[8] Supported by the National Science Foundation of China.

[9] Supported by the Danish Natural Science Research Council.

[10] Supported by the UK Particle Physics and Astronomy Research Council.

[11] Supported by the US Department of Energy, grant DE-FG0295-ER40896.

[12] Now at Departement de Physique Corpusculaire, Université de Genève, 1211 Genève 4, Switzerland.

[13] Also at Department of Physics, Tsinghua University, Beijing, P.R. China.

[14] Supported by the Leverhulme Trust.

[15] Permanent address: Universitat de Barcelona, 08208 Barcelona, Spain.

[16] Supported by Bundesministerium für Bildung und Forschung, Germany.

[17] Supported by the Direction des Sciences de la Matière, C.E.A.

[18] Supported by the Austrian Ministry for Science and Transport.

[19] Now at SAP AG, 69185 Walldorf, Germany.

[20] Now at Groupe d' Astroparticules de Montpellier, Université de Montpellier II, 34095 Montpellier, France.

[21] Now at BNP Paribas, 60325 Frankfurt am Main, Germany.

[22] Supported by the US Department of Energy, grant DE-FG03-92ER40689.

[23] Now at Institut Inter-universitaire des hautes Energies (IIHE), CP 230, Université Libre de Bruxelles, 1050 Bruxelles, Belgique.

[24] Also at Dipartimento di Fisica e Tecnologie Relative, Università di Palermo, Palermo, Italy.

[25] Deceased.

[26] Now at SLAC, Stanford, CA 94309, USA.

[27] Now at IWR, Forschungzentrum Karlsruhe, Postfach 3640, 76021 Karlsruhe, Germany.

[28] Research Fellow of the Belgium FNRS.

[29] Research Associate of the Belgium FNRS.

[30] Now at Liverpool University, Liverpool L69 7ZE, United Kingdom.

[31] Supported by the Federal Office for Scientific, Technical and Cultural Affairs through the Interuniversity Attraction Pole P5/27.

[32] Now at INP, Cracow, Poland.

[33] Now at Laboratorium für Hochenergiephysik, Universität Bern, 3012 Bern, Switzerland.

1 Introduction

Bose-Einstein correlation (BEC) leads to an enhancement of the two-particle differential cross section for bosons which are close in phase-space. First experimental evidence for BEC was reported by Goldhaber et al. [1] for $\pi^{\pm}\pi^{\pm}$ pairs produced in $\mathrm{p}\bar{\mathrm{p}}$ annihilations. Since then this phenomenon has been studied over a wide range of centre-of-mass energies for hadronic final states produced by different initial states [2–6]. BEC has become an important tool to investigate the space-time characteristics of the boson production region in hadronic events.

Previous analyses of BEC in hadronic Z decays at LEP have studied this phenomenon in terms of the two-particle correlation function $C_2(Q)$, where $Q = \sqrt{-(p_1 - p_2)^2}$ is the Lorentz-invariant four-momentum difference of a pair of particles, assuming a spherically symmetric shape of the boson emission region [7–10].

According to the Lund string model [11] this reflects only a simplified picture of the true source shape, since this model predicts a difference between the longitudinal and transverse correlation lengths with respect to the jet axis in $\mathrm{e}^+\mathrm{e}^-$ events [12]. In order to test these predictions, the shape of the BEC function has been studied by the DELPHI [13], L3 [14] and OPAL [15] collaborations using two- and three-dimensional distributions of components of Q, showing an elongation of the boson source region with respect to the jet axis.

In this paper a detailed analysis is presented of one- and two-dimensional BEC in pairs of charged pions in $\mathrm{e}^+\mathrm{e}^- \to \mathrm{Z} \to \mathrm{q}\bar{\mathrm{q}}$ events, recorded with the ALEPH detector at LEP in 1994. The results are compared with those obtained from the analysis of events simulated with JETSET [16], including BEC. A study is made of the influence of the quark flavour composition and the two-jet purity of the analysed sample. The aim of this paper is to present a statistically precise measurement of the BEC effect and to survey the influence of the analysis methods on the results.

2 The correlation function

2.1 Definition and parametrisation

In order to analyse BEC between pairs of bosons a correlation function C_2 is defined by

$$C_2(p_1, p_2) = \frac{P(p_1, p_2)}{P(p_1)P(p_2)}, \qquad (1)$$

where p_1 and p_2 are the four-momenta of the two bosons, $P(p_1, p_2)$ is the two-particle probability density function and $P(p_1)$, $P(p_2)$ represent the single particle probability densities. $P(p_1, p_2)$ corresponds to the two-particle differential cross section and can be measured experimentally, whereas the product $P(p_1)P(p_2)$ is more difficult to assess and is usually replaced by the two-particle distribution $P_0(p_1, p_2)$, which corresponds to $P(p_1)P(p_2)$ in the absence of BEC. $P_0(p_1, p_2)$ is referred to as the reference sample. The commonly used parametrisation of C_2 as a function of Q is the Goldhaber parametrisation [1, 17],

$$C_2(Q) = 1 + \lambda e^{-Q^2 R^2}, \qquad (2)$$

where λ is related to the fraction of particles which interfere and is often denoted as the coherence strength factor, meaning $\lambda = 1$ for fully incoherent and $\lambda = 0$ for fully coherent sources. The parameter R is interpreted as the radius of the source, assumed to be spherical in this parametrisation [18]. In order to describe the correlation function obtained from data a modified version of (2) is used:

$$C_2(Q) = N[1 + \lambda e^{-Q^2 R^2}][1 + \epsilon Q], \qquad (3)$$

where N is the overall normalisation factor and the linear term accounts for long-range correlations outside the region of BEC.

In order to compare the analysis results with the predictions of BEC in the Lund string model for bosons produced in $e^+e^- \to q\bar{q}$ events, C_2 has to be described as a function of components of Q in the rest frame of the string between the initial $q\bar{q}$ pair. Such a frame is the Longitudinal Centre-of-Mass System (LCMS) which is defined for each pair of particles as the coordinate system in which the momentum sum of the two particles is perpendicular to a chosen reference axis of the event [12]. The reference axis has to be a physical axis of the process which in two-jet events can be chosen as the jet direction or the direction of the primary parton in e^+e^- annihilation. In the present analysis the thrust axis was chosen as the reference axis, since in events with a two-jet topology it approximates well the direction of the initial quark pair. In the LCMS the four-momentum difference Q is decomposed into Q_L, parallel, and Q_T, perpendicular to the thrust axis. In analogy to (3) the correlation function in terms of Q_T and Q_L then reads:

$$\begin{aligned} &C_2(Q_T, Q_L) \\ &= N\left(1 + \lambda e^{-R_T^2 Q_T^2 - R_L^2 Q_L^2}\right)\left(1 + \epsilon_T Q_T + \epsilon_L Q_L\right). \end{aligned} \qquad (4)$$

2.2 Measurement of the correlation function

Experimentally the two-dimensional correlation function is obtained from the ratio of the distributions of the number of identical boson-pairs, $N^{\pm\pm}(Q_T, Q_L)$, to the number of pairs in the reference sample, $N^{\mathrm{ref}}(Q_T, Q_L)$:

$$r_{\mathrm{ref}}(Q_T, Q_L) = \frac{N^{\pm\pm}(Q_T, Q_L)}{N^{\mathrm{ref}}(Q_T, Q_L)}. \qquad (5)$$

Ideally, the reference sample must contain all features present in the distribution of like-sign pairs, except BEC, and must not contain additional correlations induced by the sample preparation. Constructing such a reference sample is the major experimental problem in this kind of analysis.

A common method to obtain the reference sample is to pair bosons of the same kind but with opposite electric charge, which is referred to as the unlike-sign reference sample. The main disadvantage of this kind of reference sample is the inclusion of correlations due to resonance decays in the distribution of the number of unlike-sign pairs, $N^{+-}(Q_T, Q_L)$.

Another frequently used method is the event-mixing method, i.e. a mixed reference sample, $N^{\mathrm{mix}}(Q_T, Q_L)$, is constructed, where the same kind of particles stemming from different events with similar topological and kinematical structure are paired. In the present analysis the mixed reference sample was constructed in the following way: first, all events are rotated to a coordinate system which has the z-axis along the thrust axis. A buffer of M events is created and each track from the current event is paired with a randomly chosen track from each event in the buffer. The buffer size, $M = 17$, was chosen according to the average charged track multiplicity of the data sample. For each new current event the buffer is updated. Of course, the event-mixing method removes not only BEC, but also other correlations such as kinematical correlations.

It is important to note that the two methods employed in this analysis to obtain the reference sample represent rather extreme cases in terms of correlations: while the event-mixing method removes further correlations than just BEC, the unlike-sign method induces additional unwanted correlations.

To correct for the inadequacies of the reference sample and for detector acceptance effects the ratio $r_{\mathrm{ref}}^{\mathrm{MC}}(Q_T, Q_L)$ is computed using a sample of Monte Carlo events without BEC simulation included. The measured two-particle correlation function $C_2(Q_T, Q_L)$ is then obtained from the double-ratio:

$$C_2^{+-}(Q_T, Q_L) = \frac{r_{+-}^{\mathrm{data}}(Q_T, Q_L)}{r_{+-}^{\mathrm{MC}}(Q_T, Q_L)}$$

and $\qquad (6)$

$$C_2^{\mathrm{mix}}(Q_T, Q_L) = \frac{r_{\mathrm{mix}}^{\mathrm{data}}(Q_T, Q_L)}{r_{\mathrm{mix}}^{\mathrm{MC}}(Q_T, Q_L)},$$

where the subscripts "$+-$" and "mix" refer to the different kind of reference samples. The four distributions, $N_{\mathrm{data}}^{\pm\pm}$, $N_{\mathrm{MC}}^{\pm\pm}$, $N_{\mathrm{data}}^{\mathrm{ref}}$, $N_{\mathrm{MC}}^{\mathrm{ref}}$, needed to compute the two-dimensional

correlation function (6), were filled into two-dimensional histograms. Taking into account the available statistics and the resolution in Q, estimated from the simulation, a bin size of 40 MeV/c was chosen. The same procedure was applied to obtain the one-dimensional correlation function, $C_2(Q)$, except that in this case the distributions are accumulated in 20 MeV/c bins of the Lorentz-invariant four-momentum difference Q.

3 The ALEPH detector

The ALEPH detector is described in detail in [19] and its performance in [20]. The tracking system consists of two layers of double-sided silicon vertex-detectors (VDET), an inner tracking chamber (ITC) and a time projection chamber (TPC). The VDET single hit resolution is $12\,\mu m$ at normal incidence for both the $r\phi$ and rz projections and $22\,\mu m$ at maximum polar angle. The polar angle coverage of the inner and outer layers are $|\cos\theta| < 0.84$ and $|\cos\theta| < 0.69$ respectively. The ITC provides up to 8 $r\phi$ hits at radii 16 to 26 cm relative to the beam with an average resolution of $150\,\mu m$ and has an angular coverage of $|\cos\theta| < 0.97$. The TPC measures up to 21 space points per track at radii between 38 and 171 cm, with an $r\phi$ resolution of $170\,\mu m$ and a z resolution of $740\,\mu m$ and with an angular coverage of $|\cos\theta| < 0.96$. In addition, the TPC wire planes provide up to 338 samples of ionisation energy loss (dE/dx).

The TPC, ITC and VDET are immersed in a 1.5 T axial magnetic field. Combined they provide a transverse momentum resolution of $\sigma(1/p_T) = 0.0006\,(\text{GeV}/c)^{-1}$ for 45 GeV muons. Multiple scattering dominates at low momentum and adds a constant term of 0.005 to $\sigma(p_T)/p_T$.

Outside of the TPC, the electromagnetic calorimeter (ECAL) consists of 45 layers of lead interleaved with proportional wire chambers. The ECAL is used to identify photons and electrons and gives an energy resolution $\sigma(E)/E = 0.18/\sqrt{E/\text{GeV}} + 0.009$ for isolated particles. The hadron calorimeter (HCAL) is formed by the iron of the magnet return yoke interleaved with 23 layers of streamer tubes. It is used to measure hadronic energy and, together with two surrounding layers of muon chambers, to identify muons.

The information from the subdetectors is combined in an energy flow algorithm [20] which gives a list of charged and neutral track momenta.

4 Data selection

In this analysis data accumulated in 1994 with the ALEPH detector at centre-of-mass energies around $\sqrt{s} =$91.2 GeV were used.

Only charged tracks in hadronic events were considered. The non-hadronic background was reduced by selecting only events which contained at least eight charged tracks with at least 10% of the total centre-of-mass energy. Events inside the acceptance region of the tracking system were selected by requiring $|\cos(\theta_{\text{thrust}})| < 0.9$, where θ_{thrust} is the polar angle of the thrust axis.

In order to perform the mixing procedure correctly only two-jet events were selected by requiring events with a thrust value above 0.95. This selection also makes the definition of the LCMS unambiguous, since the line of flight of the initial quarks in $e^+e^- \rightarrow q\bar{q}$ events is then, to a good approximation, represented by the thrust axis. From the initial $2 \cdot 10^6$ events a total of about $8.5 \cdot 10^5$ events fulfilled these selection criteria.

The tracking performance of the detector is of great importance for this analysis, which requires an accurate track reconstruction and good separation of nearby tracks with small relative momenta. The high quality of reconstructed tracks was guaranteed by requiring at least six hits in the TPC and a polar angle, θ, with $|\cos(\theta)| < 0.95$. Since the high voltage membrane inside the TPC is perpendicular to the beam axis and goes through the origin of the coordinate system, tracks which are nearly perpendicular to the beam axis are likely to be split into multiple tracks with small relative momenta. Therefore, tracks with θ values between $89°$ and $91°$ were disregarded.

Pairs of particles with at least one partner not produced during hadronisation reduce the strength of the measured BEC effect. Therefore, the number of secondary particles stemming from long-lived decays, nuclear interactions and fake tracks, was reduced by setting the maximum allowed distance to the interaction vertex to 2 mm in the xy-plane and to 6 mm in the z direction.

Remaining charged tracks which were identified as originating from decay products of neutral particles, V^0's (e.g. K^0_s and Λ), and tracks from nuclear interactions with detector material were also rejected [20]. Electrons from photon conversions and Dalitz pairs were rejected by requiring tracks with a measured dE/dx within four standard deviations of that expected for a pion and more than three standard deviations away from the one expected for an electron. To avoid kinematic correlations, which appear in the limit of the allowed phase-space, only tracks with a momentum smaller than 4.5 GeV/c were selected.

All tracks that passed these selection criteria were assumed to be pions. Separation of K/π by means of the specific energy loss by ionisation was not considered, since the cross-over region of the respective Bethe-Bloch curves lies in the allowed momentum range of the selected tracks. However, the Monte Carlo simulation indicates that only 7.7% of the analysed tracks correspond to kaon tracks.

Pairs of like-sign tracks with an opening angle, θ_{12}, smaller than $2°$ are likely not to be resolved by the TPC and were rejected. According to the simulation, 76% of the selected track pairs are pion pairs.

Unless stated otherwise, all Monte Carlo events used in the analysis were generated without BEC nor final-state Coulomb and strong interaction between hadrons moving away from the hadronisation region, using JETSET 7.4 with ALEPH tuning [21].

5 One-dimensional BEC

5.1 Results

The measured correlation functions, $C_2^{+-}(Q)$ and $C_2^{\text{mix}}(Q)$, obtained using ALEPH data, are shown in Fig. 1 for the
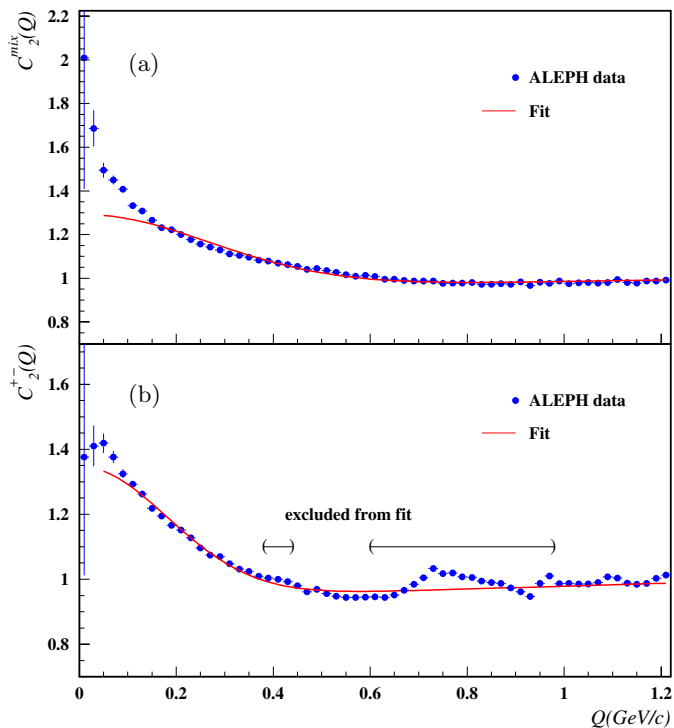
Fig. 1. The one-dimensional correlation function measured with ALEPH data using **a** the mixed reference sample, $C_2^{\mathrm{mix}}(Q)$; **b** the unlike-sign reference sample, $C_2^{+-}(Q)$. The fit of (3) is superimposed

region $Q < 1.2\,\mathrm{GeV/c}$. The bin size of Fig. 1 is $20\,\mathrm{MeV/c}$, to be compared with a typical resolution in Q of $5\,\mathrm{MeV/c}$.

In both measurements a clear enhancement for $Q \lesssim 0.4\,\mathrm{GeV/c}$ due to BEC can be observed. The superimposed curve in Fig. 1 is the result of the fit to the Goldhaber parametrisation, (3), in the region $0.04 < Q < 2\,\mathrm{GeV/c}$. The region $Q < 40\,\mathrm{MeV/c}$ was excluded from the fit since in this region the effects of Coulomb and strong interaction, not included in the simulation, become important.

As a consequence of imperfections in the modelling of the K_S^0 and the ρ^0 resonance in the simulation, the regions of the $C_2^{+-}(Q)$ distribution sensitive to those particles cannot be eliminated by taking the double ratio in (6). These regions, $0.6 < Q < 0.98\,\mathrm{GeV/c}$ and $0.38 < Q < 0.44\,\mathrm{GeV/c}$, were excluded from the fit of $C_2^{+-}(Q)$.

The χ^2/ndf values in Table 1 show that (3) does not describe the data. The slope of the solid curves for $Q \lesssim 0.2\,\mathrm{GeV/c}$ in Fig. 1 indicates that a Gaussian source shape can only be regarded as a first approximation. The resulting numerical values of the fitted parameters given in Table 1 will be referred to as the "reference values" throughout the discussion of the one-dimensional analysis. The correlation between λ and R is $+92\%$ for C_2^{mix} and $+68\%$ for C_2^{+-}.

The large discrepancy between the λ and R values estimated from the two methods reflects the strong influence of the chosen reference sample on the analysis results. In order to check how the excluded regions influence the results, $C_2^{\mathrm{mix}}(Q)$ was also fitted with the same exclusion regions as in the fit of $C_2^{+-}(Q)$, which resulted in a negligible effect on the fitted parameter values.

Table 1. The reference values obtained from the fit of (3) to $C_2^{\mathrm{mix}}(Q)$ and $C_2^{+-}(Q)$

	$C_2^{\mathrm{mix}}(Q)$	$C_2^{+-}(Q)$
N	0.948 ± 0.001	0.936 ± 0.001
λ	0.362 ± 0.006	0.438 ± 0.006
R (fm)	0.528 ± 0.005	0.777 ± 0.007
ϵ (fm)	$(0.768 \pm 0.010) \cdot 10^{-2}$	$(0.905 \pm 0.002) \cdot 10^{-2}$
χ^2/ndf	$513 \ / \ 94$	$432 \ / \ 72$

5.2 Study of systematic effects

5.2.1 Track selection

The systematic effects related to the track selection criteria were estimated by repeating the analysis with a modified set of selection cuts. The influence of the maximum allowed track momentum was investigated by repeating the analysis for tracks with $p < 3.5\,\mathrm{GeV/c}$, $p < 4\,\mathrm{GeV/c}$, $p < 5\,\mathrm{GeV/c}$ and $p < 5.5\,\mathrm{GeV/c}$. The systematic uncertainty resulting from the variation of this selection cut was taken as the root mean square (RMS) of the deviation from the reference values. Likewise, the systematic uncertainty resulting from the variation of the minimum allowed θ_{12} was repeated for $\theta_{12} > 0°$ and $\theta_{12} > 3°$. The largest systematic uncertainty on λ, related to the track selection criteria, resulted from increasing the distance of closest approach to the interaction vertex to $2\,\mathrm{cm}$ in the xy-plane and to $10\,\mathrm{cm}$ along the z direction, which yields an uncertainty of 5% when using the mixed and of 7% when using the unlike-sign reference sample. Other systematic effects related to the track selection criteria were investigated by selecting tracks with four TPC hits, or by removing one selection cut at a time, such as the e^- rejection, the cut on the polar angle, $89° < \theta < 91°$, or the V^0 rejection. The largest uncertainty on the source radius, R, obtained with the mixed reference sample, is due to the e^- rejection cut, 4%. The systematic effects related to the track selection criteria have only an effect of less than 2% on the radius R when using the unlike-sign reference sample.

In order to include the systematic effects due to the finite detector resolution in Q, the analysis was repeated using a bin width of $50\,\mathrm{MeV/c}$. The influence of long-range correlations was estimated by varying the upper limit of the fit range, $Q_{\max}$, between $1.8\,\mathrm{GeV/c}$ and $2\,\mathrm{GeV/c}$. The largest deviation from the reference values, resulting from this variation, was taken as the corresponding uncertainty, yielding an effect of the order of 2% and 1% for the unlike-sign and the mixed reference sample, respectively. The total systematic uncertainty related to the effects presented in this subsection was computed by adding all the contributions in quadrature. This yielded $\Delta\lambda = 0.032$, $\Delta R = 0.026$ fm for the parameter values obtained using the mixed reference sample. Using the unlike-sign reference sample the total systematic uncetainty is $\Delta\lambda = 0.046$ and $\Delta R = 0.033$ fm.

5.2.2 Analysis procedure

There are sources of systematic effects which are introduced by the choice of the reference sample. The only free

parameter in the mixing procedure used in this analysis is the chosen buffer size, M. The systematic uncertainty related to this parameter was accounted for by repeating the analysis for $18 \leq M \leq 30$ and taking the RMS of the deviation from the reference values, yielding an uncertainty of less than 1%, $\Delta\lambda = 0.003$ and $R = 0.006$ fm.

A source of systematic effects which is only related to the unlike-sign reference sample is the choice of the excluded regions from the fit. The corresponding systematic uncertainty was estimated by repeating the fit with different choices of the excluded regions, for each of the two regions separately: the range of the K_S^0 peak was varied between [0.34, 0.44] GeV/c and [0.38,0.46] GeV/c; the range of the ρ^0 resonance between [0.66,0.96] GeV/c and [0.56,1.00] GeV/c. The largest deviation of the thus obtained parameter values from the reference values was taken as the systematic uncertainty, giving 2% for the K_S^0 region, $\Delta\lambda = 0.010$ and $\Delta R = 0.012$ fm. The variation of the ρ^0 resonance region yielded an uncertainty $\Delta\lambda = 0.008$ and $\Delta R = 0.024$ fm.

5.2.3 Quark flavour composition

Due to the long lifetime and large mass of b-hadrons, their decays are characterised by many decay products with large impact parameter, defined as the distance of closest approach between a daughter track and the b production point. Pions stemming from such decays are likely to be paired with a pion produced during the hadronisation phase and hence reduce the fraction of pion-pairs which are subject to BEC. The influence of the uds-purity of the analysed sample on the measured correlation function, $C_2^{\mathrm{mix}}(Q)$, was studied using a b-tagging algorithm [22]. As a consequence λ was found to increase with uds-purity, from $\lambda = 0.362 \pm 0.006$ (reference value) with an uds-purity of 61% to $\lambda = 0.497 \pm 0.006$ with an uds-purity of 82%. In contrast to this, the measured source radius, R, which is the most interesting parameter in this analysis, remained fairly constant.

5.3 Monte Carlo studies

In the data a systematic difference is observed between results obtained with the two kinds of reference samples. Detailed analyses of BEC in Monte Carlo generators have been presented in previous papers [23, 24]. In this paper Monte Carlo studies of BEC have been included in order to further investigate in which way the reference sample influences the results. For this study a sample of $4.75 \cdot 10^5$ events generated with JETSET was used. Bose-Einstein effects are simulated in JETSET in such a way as to reproduce the shape of the two-particle correlation function according to $C_2(Q) = 1 + \lambda_{\mathrm{input}} e^{-(QR_{\mathrm{input}})^2}$, where λ_{input} and R_{input} are the input parameters. Their values, $\lambda_{\mathrm{input}} = 1.12$ and $R_{\mathrm{input}} = 0.595$ fm, were taken from a global fit to the PYBOEI [25] model implemented in the PYTHIA Monte Carlo generator [16], version 6.1. The global fit of free parameters of the model, including both the BEC parameters

and the QCD parameters, was made to the hadronic Z data used in the present analysis.

The measured correlation functions, $C_{2,\mathrm{MC+BEC}}^{+-}(Q)$ and $C_{2,\mathrm{MC+BEC}}^{\mathrm{mix}}(Q)$, were obtained according to (6). In order to better extract the characteristics of the BEC simulation in JETSET, without the effects introduced by the mixed and the unlike-sign reference samples, the correlation function was also estimated from the ratio:

$$R_{2,\mathrm{MC+BEC}}(Q) = \frac{N_{\mathrm{MC+BEC}}^{\pm\pm}(Q)}{N_{\mathrm{MCnoBEC}}^{\pm\pm}(Q)} \qquad (7)$$

The correlation functions obtained from the JETSET sample are shown in Fig. 2, together with the fit of (3). In order to compare these results with the ones obtained from data, the same fit regions (excluding the same regions in the fit of $C_{2,\mathrm{MC+BEC}}^{+-}(Q)$) as in the previous fits were used.

The resulting distributions of the three correlation functions, shown in Fig. 2, are qualitatively compatible with the ones obtained from the ALEPH data (Fig. 1): an enhancement is observed for $Q \lesssim 0.4$ GeV/c and a slope larger than that expected for a Gaussian for $Q \lesssim 0.2$ GeV/c. As in the data, the result depends on the choice of reference sample.

In agreement with [26], the comparison of the results of the fitted parameters in Table 2 with the input parameters, λ_{input} and R_{input}, shows that the fit of (3) to the correlation function does not yield the chosen input parameter values used in the analysed JETSET sample. This is also observed in the case where the correlation function is obtained from the single ratio, (7), which indicates that this outcome is a feature of the particular implementation of BEC in JETSET.
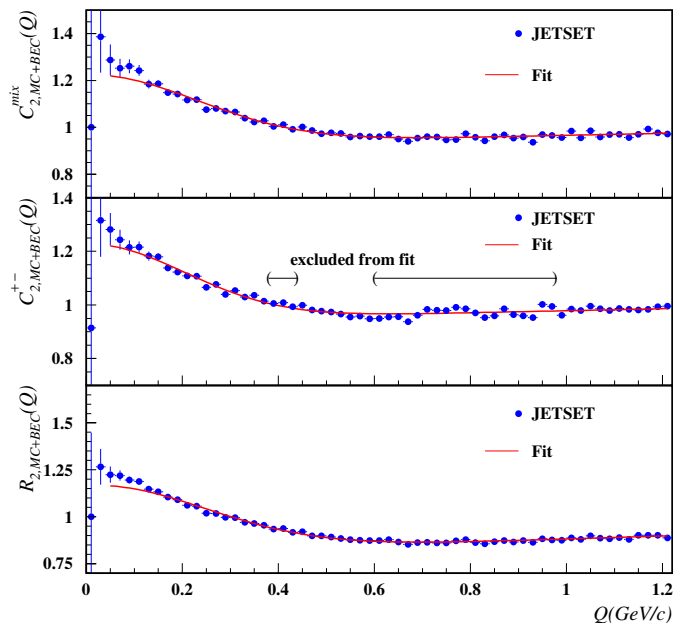

Fig. 2. The one-dimensional correlation function measured in events generated with JETSET 7.4, including BEC simulation. The fit of (3) is superimposed

Table 2. The values obtained from the fit of (3) to the correlation function in the Monte Carlo simulation

	$C_{2,\mathrm{MC+BEC}}^{\mathrm{mix}}(Q)$	$C_{2,\mathrm{MC+BEC}}^{+-}(Q)$	$R_{2,\mathrm{MC+BEC}}(Q)$
N	0.923 ± 0.013	1.158 ± 0.002	0.804 ± 0.001
λ_{input}	1.120	1.120	1.120
λ	0.325 ± 0.032	0.252 ± 0.006	0.451 ± 0.004
R_{input} (fm)	0.595	0.595	0.595
R (fm)	0.611 ± 0.075	0.695 ± 0.012	0.574 ± 0.001
δ (fm)	$(0.912 \pm 0.225) \cdot 10^{-2}$	$(0.455 \pm 0.032) \cdot 10^{-2}$	$(0.190 \pm 0.003) \cdot 10^{-1}$
χ^2/ndf	104 / 94	94 / 72	133 / 94

6 Two-dimensional BEC

6.1 Results

The measured two-dimensional correlation functions, $C_2^{\mathrm{mix}}(Q_{\mathrm{T}}, Q_{\mathrm{L}})$ and $C_2^{+-}(Q_{\mathrm{T}}, Q_{\mathrm{L}})$, are shown in Fig. 3. It should be noted that the histograms shown in Fig. 3 have a coarser binning ($100 \, \mathrm{MeV}/c$) than the ones used in the analysis. The result of the fit of (4) in the region $0.04 \, \mathrm{GeV}/c < Q_{\mathrm{T}}, |Q_{\mathrm{L}}| < 1.2 \, \mathrm{GeV}/c$ is displayed in Figs. 3c–f, together with the projections of C_2 onto the Q_{T} and Q_{L} axes. In order to avoid the regions of $C_2^{+-}(Q_{\mathrm{T}}, Q_{\mathrm{L}})$ sensitive to the $\mathrm{K}_{\mathrm{S}}^0$ and the ρ^0 resonance, the ranges $0.38 \, \mathrm{GeV}/c < \sqrt{Q_{\mathrm{T}}^2 + Q_{\mathrm{L}}^2} < 0.44 \, \mathrm{GeV}/c$ and $0.6 \, \mathrm{GeV}/c < \sqrt{Q_{\mathrm{T}}^2 + Q_{\mathrm{L}}^2} < 0.98 \, \mathrm{GeV}/c$ were excluded from the fit of $C_2^{+-}(Q_{\mathrm{T}}, Q_{\mathrm{L}})$. In the following discussion of the two-dimensional analysis the parameter values resulting from this fit (Table 3) will be referred to as the "reference values".

As predicted by the Lund string model [11], a difference between the transverse, R_{T}, and the longitudinal correlation radius, R_{L}, is observed. This is an indication for an elongation of the pion emission region, with respect to the jet axis. The correlation between R_{T} and R_{L}, $+29\%$ for C_2^{mix} and $+20\%$ for C_2^{+-}, is taken into account in the statistical error of $R_{\mathrm{T}}/R_{\mathrm{L}}$.

A large discrepancy is seen between the fitted parameter values obtained using the mixed and the unlike-sign reference samples. As seen in Table 3 and from the comparison with previous results [13–15] the BEC parameter values obtained using the unlike-sign reference sample tend to be larger than the ones obtained with the mixed reference sample.

Table 3. Reference values obtained from the fit of (4) to $C_2^{\mathrm{mix}}(Q_{\mathrm{T}}, Q_{\mathrm{L}})$ and $C_2^{+-}(Q_{\mathrm{T}}, Q_{\mathrm{L}})$

	$C_2^{\mathrm{mix}}(Q_{\mathrm{T}}, Q_{\mathrm{L}})$	$C_2^{+-}(Q_{\mathrm{T}}, Q_{\mathrm{L}})$
N	1.033 ± 0.002	0.992 ± 0.002
λ	0.310 ± 0.005	0.384 ± 0.007
R_{T} (fm)	0.470 ± 0.007	0.788 ± 0.010
R_{L} (fm)	0.767 ± 0.011	0.870 ± 0.019
$\frac{R_{\mathrm{T}}}{R_{\mathrm{L}}}$	0.612 ± 0.010	0.906 ± 0.020
ϵ_{T} (fm)	$(-0.139 \pm 0.004) \cdot 10^{-1}$	$(-0.421 \pm 0.064) \cdot 10^{-2}$
ϵ_{L} (fm)	$(-0.614 \pm 0.227) \cdot 10^{-3}$	$0.113 \cdot 10^{-9} \pm 0.118 \cdot 10^{-2}$
χ^2/ndf	2297 / 1792	1810 / 1158

Table 4. Parameter values obtained from the fit of the Edgeworth expansion (8) to $C_2^{\mathrm{mix}}(Q_{\mathrm{T}}, Q_{\mathrm{L}})$ and $C_2^{+-}(Q_{\mathrm{T}}, Q_{\mathrm{L}})$

	$C_2^{\mathrm{mix}}(Q_{\mathrm{T}}, Q_{\mathrm{L}})$	$C_2^{+-}(Q_{\mathrm{T}}, Q_{\mathrm{L}})$
N	1.010 ± 0.002	1.015 ± 0.004
λ	0.337 ± 0.005	0.361 ± 0.007
R_{T} (fm)	0.505 ± 0.009	0.779 ± 0.010
R_{L} (fm)	0.746 ± 0.012	0.929 ± 0.022
$\frac{R_{\mathrm{T}}}{R_{\mathrm{L}}}$	0.677 ± 0.013	0.839 ± 0.020
ϵ_{T} (fm)	$(-0.324 \pm 0.073) \cdot 10^{-2}$	$(-0.159 \pm 0.016) \cdot 10^{-1}$
ϵ_{L} (fm)	$(-0.158 \pm 0.041) \cdot 10^{-2}$	$(-0.017 \pm 0.268) \cdot 10^{-3}$
κ_{T}	$(-0.648 \pm 0.042) \cdot 10^{-2}$	$(0.161 \pm 0.020) \cdot 10^{-2}$
κ_{L}	$(0.300 \pm 0.105) \cdot 10^{-3}$	$0.165 \cdot 10^{-6} \pm 0.205 \cdot 10^{-3}$
χ^2/ndf	2186 / 1792	1765 / 1158

Both reference samples yield large χ^2/ndf values (Table 3), indicating that the shape of the pion source is not well described by the two-dimensional Goldhaber parametrisation, similar to the one-dimensional case.

A slightly better fit quality was obtained by using the Edgeworth expansion as described in [14]:

$$C_2 = N \left(1 + \lambda e^{-R_{\mathrm{T}}^2 Q_{\mathrm{T}}^2 - R_{\mathrm{L}}^2 Q_{\mathrm{L}}^2}\right) (1 + \epsilon_{\mathrm{T}} Q_{\mathrm{T}} + \epsilon_{\mathrm{L}} Q_{\mathrm{L}})$$
$$\times \left[1 + \frac{\kappa_{\mathrm{L}}}{3!} H_3 (R_{\mathrm{L}} Q_{\mathrm{L}})\right] \left[1 + \frac{\kappa_{\mathrm{T}}}{3!} H_3 (R_{\mathrm{T}} Q_{\mathrm{T}})\right], \quad (8)$$

where κ_i ($i = \mathrm{L}, \mathrm{T}$) is the third-order cumulant moment in the corresponding direction and $H_3(R_i Q_i) = (\sqrt{2} R_i Q_i)^3 - 3\sqrt{2} R_i Q_i$ is the third order Hermite polynomial. The systematic differences between the results obtained from the two kinds of reference samples remain (cf. Table 4).

6.2 Study of systematic effects

In order to take into account correlations between R_{T} and R_{L}, the systematic uncertainty of $R_{\mathrm{T}}/R_{\mathrm{L}}$ was estimated with respect to the result of the fit with a modified version of (4), where $R_{\mathrm{T}}/R_{\mathrm{L}}$ is taken as the complementary parameter to R_{L}:

$$C_2 (Q_T, Q_L) = N \left(1 + \lambda e^{-R_{\mathrm{L}}^2 \left((R_{\mathrm{T}}^2/R_{\mathrm{L}}^2)Q_T^2 + Q_L^2\right)}\right)$$
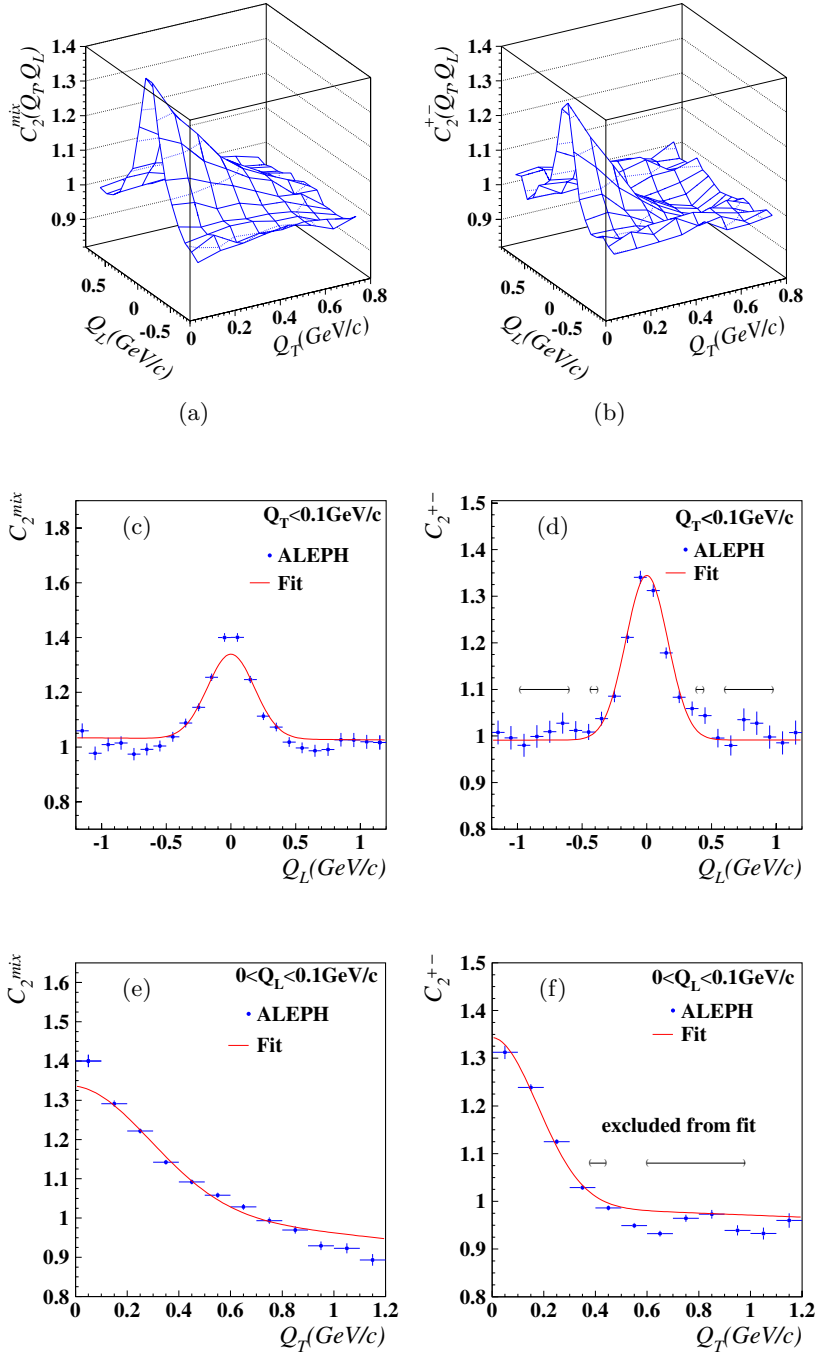$$\times (1 + \epsilon_{\mathrm{T}} Q_{\mathrm{T}} + \epsilon_{\mathrm{L}} Q_{\mathrm{L}}). \quad (9)$$

Fig. 3. The measured two-dimensional correlation function **a** obtained using the mixed reference sample, $C_2^{mix}(Q_T, Q_L)$ and its projection onto **c** the Q_L and **e** the Q_T axes; **b** obtained using the unlike-sign reference sample, $C_2^{+-}(Q_T, Q_L)$ and its projection onto **d** the Q_L and **f** the Q_T axes

The fit to (9), performed in the same regions used for the computation of the reference values, yields $R_T/R_L = 0.612 \pm 0.012$, $R_L = 0.767 \pm 0.012$ fm for C_2^{mix} and $R_T/R_L = 0.906 \pm 0.010$, $R_L = 0.870 \pm 0.008$ fm for C_2^{+-}, which is consistent with the reference values.

6.2.1 Track selection

In analogy to the one-dimensional analysis the systematic uncertainty was estimated by varying the selection criteria as described in Sect. 5.2. The largest thus estimated systematic effect resulted from the variation of the allowed momentum range, 2% on R_T, 3.6% on R_L and 3.4% on R_T/R_L when using the mixed reference sample. Similarly, the most important contributions to the systematic uncertainty on the parameters obtained from $C_2^{+-}(Q_T, Q_L)$ come from the variation of the minimum allowed θ_{12} value, 2% on R_T, 1% on R_L and R_T/R_L, from accepting tracks with at least four hits in the TPC, 2% on R_T, R_L and R_T/R_L, and from the e^- rejection cut, 1% on R_T and R_L and 2% on R_T/R_L.

Table 5. The parameter values resulting from the fit of the correlation function as measured from a JETSET sample with BEC simulation included

	$C_{2,\mathrm{MC+BEC}}^{\mathrm{mix}}(Q_\mathrm{T}, Q_\mathrm{L})$	$C_{2,\mathrm{MC+BEC}}^{+-}(Q_\mathrm{T}, Q_\mathrm{L})$	$R_{2,\mathrm{MC+BEC}}(Q_\mathrm{T}, Q_\mathrm{L})$
N	0.938 ± 0.005	0.975 ± 0.006	0.790 ± 0.003
λ_{input}	1.12	1.12	1.12
λ	0.298 ± 0.011	0.263 ± 0.012	0.478 ± 0.008
R_{input} (fm)	0.595	0.595	0.595
R_T (fm)	0.527 ± 0.018	0.651 ± 0.028	0.502 ± 0.007
R_L (fm)	0.621 ± 0.023	0.682 ± 0.039	0.615 ± 0.010
$\left(\frac{R_\mathrm{T}}{R_\mathrm{L}}\right)_{\mathrm{input}}$	1	1	1
$\frac{R_\mathrm{T}}{R_\mathrm{L}}$	0.848 ± 0.038	0.955 ± 0.055	0.816 ± 0.016
ϵ_T (fm)	$(0.617 \pm 0.140) \cdot 10^{-2}$	$(0.038 \pm 0.158) \cdot 10^{-2}$	0.033 ± 0.001
ϵ_L (fm)	$(0.326 \pm 0.478) \cdot 10^{-3}$	$0.606 \cdot 10^{-11} \pm 0.131 \cdot 10^{-3}$	$(0.484 \pm 0.312) \cdot 10^{-3}$
χ^2/ndf	$1839 \ / \ 1792$	$1199 \ / \ 1158$	$1994 \ / \ 1792$

The contribution to the systematic uncertainty due to the resolution in Q was estimated by increasing the bin size to $100\,\mathrm{MeV}/c$ which gave no relevant contribution.

The total systematic uncertainty related to the effects discussed here, was computed by adding all the contributions in quadrature. This yielded $\Delta\lambda = 0.030$, $\Delta R_\mathrm{T} = 0.020$ fm, $\Delta R_\mathrm{L} = 0.040$ fm and $\Delta R_\mathrm{T}/R_\mathrm{L} = 0.028$ for the parameters obtained from C_2^{mix}. The computation of the total systematic uncertainty of the parameters obtained from C_2^{+-} yielded $\Delta\lambda = 0.043$, $\Delta R_\mathrm{T} = 0.018$ fm, $\Delta R_\mathrm{L} = 0.030$ fm and $\Delta R_\mathrm{T}/R_\mathrm{L} = 0.033$

6.2.2 Analysis procedure

The systematic uncertainty related to the buffer size was taken as the RMS of the deviations from the reference values when using buffer sizes $18 \leq M \leq 30$. This yielded an uncertainty of $\Delta\lambda = 0.004$, $\Delta R_\mathrm{T} = 0.005$ fm, $\Delta R_\mathrm{L} = 0.023$ fm and $\Delta R_\mathrm{T}/R_\mathrm{L} = 0.014$.

The effect of the regions sensitive to the $\mathrm{K_S^0}$ and the ρ^0 resonance in the case of $C_2^{+-}(Q_\mathrm{T}, Q_\mathrm{L})$ was investigated by repeating the fit with new exclusion regions, $Q \notin \{[0.34, 0.44] \ldots [0.38, 0.46]\} \,\mathrm{GeV}/c$ and $Q \notin \{[0.66, 0.96] \ldots [0.56, 1.00]\} \,\mathrm{GeV}/c$, where $Q = \sqrt{Q_\mathrm{T}^2 + Q_\mathrm{L}^2}$. The largest deviation of the thus obtained parameter values from the reference values was taken as systematic uncertainty. From the variation of the region about the $\mathrm{K_S^0}$ peak an uncertainty $\Delta\lambda = 0.002$, $\Delta R_\mathrm{T} = 0.004\,\mathrm{fm}$, $\Delta R_\mathrm{L} = 0.015\,\mathrm{fm}$ and $\Delta R_\mathrm{T}/R_\mathrm{L} = 0.020$ turns out. The variation of the ρ^0 resonance region gives an uncertainty $\Delta\lambda = 0.006$ $\Delta R_\mathrm{T} = 0.012\,\mathrm{fm}$, $\Delta R_\mathrm{L} = 0.031\,\mathrm{fm}$ and $\Delta R_\mathrm{T}/R_\mathrm{L} = 0.017$.

6.2.3 Quark flavour composition

The influence of the uds-purity was investigated in analogy to Sect. 5.2.3, using a b-tagging algorithm [22]. For this study only the correlation function as measured with the mixed reference sample was considered. The results of this investigation are in good agreement with the findings

presented in Sect. 5.2.3: the parameter λ increases with uds-purity, while the correlation radii, R_T and R_L, remain fairly constant.

6.3 Monte Carlo studies

In analogy to Sect. 5.3 the correlation function was measured using a sample of $4.75 \cdot 10^5$ events, generated with JETSET with BEC simulation turned on, with input parameters $\lambda_{\mathrm{input}} = 1.12$, $R_{\mathrm{T,input}} = R_{\mathrm{L,input}} = 0.595$ fm. The algorithm implemented in JETSET to simulate BEC assumes $(R_\mathrm{T}/R_\mathrm{L})_{\mathrm{input}} = 1$.

The results of the fit of (4) to $C_{2,\mathrm{MC+BEC}}^{\mathrm{mix}}(Q_\mathrm{T}, Q_\mathrm{L})$, $C_{2,\mathrm{MC+BEC}}^{+-}(Q_\mathrm{T}, Q_\mathrm{L})$ and $R_{2,\mathrm{MC+BEC}}(Q_\mathrm{T}, Q_\mathrm{L})$ are given in Table 5. The fit regions are the same as those used for the computation of the reference values.

It turns out that, although the BEC algorithm assumes a spherically symmetric emission region, the fit of $C_{2,\mathrm{MC+BEC}}^{\mathrm{mix}}(Q_\mathrm{T}, Q_\mathrm{L})$ yields $R_\mathrm{T}/R_\mathrm{L} < 1$. The fact that also in the case of $R_{2,\mathrm{MC+BEC}}(Q_\mathrm{T}, Q_\mathrm{L})$ the ratio $R_\mathrm{T}/R_\mathrm{L}$ is smaller than unity indicates that the difference between the correlation radii must be attributed to the particular mechanism used to simulate BEC in JETSET, cf. [27].

6.4 BEC parameters as a function of the two-jet purity

In order to explore the relevance of the two-jet purity, which is determined by selecting only events with thrust values larger than a chosen cut-off value, $T > T_{\mathrm{cut}}$, the correlation functions $C_2^{\mathrm{mix}}(Q_\mathrm{T}, Q_\mathrm{L})$ and $C_2^{+-}(Q_\mathrm{T}, Q_\mathrm{L})$ were measured with T_{cut} varied between 0.90 and 0.97. The outcome of this survey, displayed in Fig. 4, is a further confirmation of the systematic difference between the results obtained using the mixed and the unlike-sign reference sample. The results obtained from $C_2^{\mathrm{mix}}(Q_\mathrm{T}, Q_\mathrm{L})$ in Figs. 4(a) and 4(b) show that R_T falls with T_{cut}, and that R_L fluctuates within 4%. As a consequence, $R_\mathrm{T}/R_\mathrm{L}$ decreases with T_{cut} (Fig. 4(c)). On the other hand, the correlation radii obtained from $C_2^{+-}(Q_\mathrm{T}, Q_\mathrm{L})$ as a function of T_{cut} behave differently: while
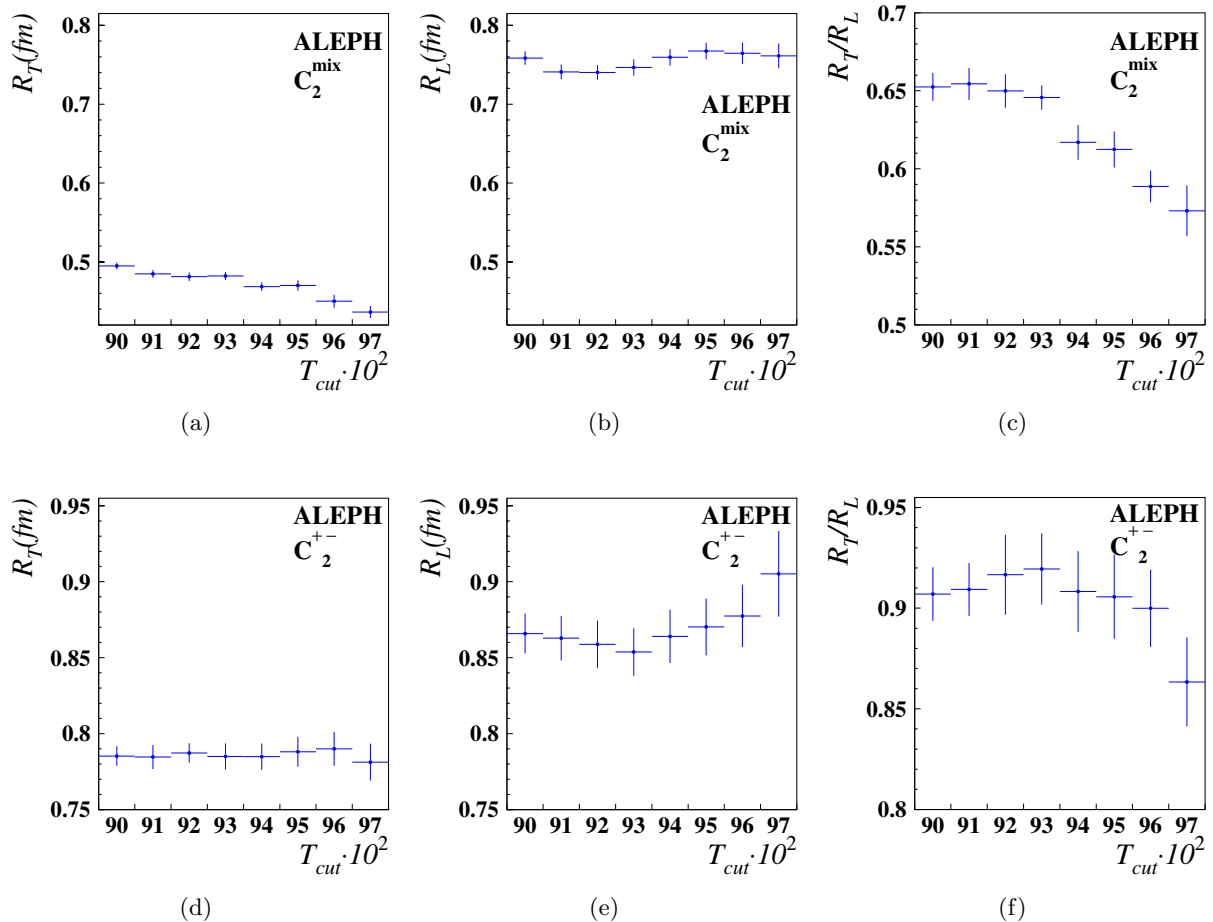
Fig. 4a–f. The correlation radii R_T and R_L and the corresponding ratio R_T/R_L as a function of the two-jet purity

R_T remains constant, R_L increases with $T_{cut} > 0.93$. In addition, the influence of the two-jet purity on the correlation radii, as obtained from $R_{2,MC+BEC}(Q_T, Q_L)$, was investigated. It turned out that R_T stays constant with $T_{cut} \leq 0.92$ and then starts to increase linearly. On the other hand, R_L has a plateau with $T_{cut} \leq 0.94$ and then decreases linearly.

7 Conclusions

A statistically precise measurement of the Bose-Einstein correlation (BEC) function for pairs of charged pions is presented. The results of the fit of the Goldhaber parametrisation to the measured correlation functions, obtained using the mixed and the unlike-sign reference samples, are given in Table 6 for events with thrust $T > 0.95$. In both cases the fit quality is poor, which indicates that a single-variable Gaussian distribution represents only a rough approximation of the shape of the charged pion emission region.

The results of the one-dimensional analyses published by the ALEPH [7], DELPHI [8], L3 [9] and OPAL [10] collaborations are listed in Table 6. The values for the correlation radius, R, agree qualitatively with respect to the same kind of reference sample. Less agreement is observed

between the different values for the coherence strength factor, λ, that depends on the purity of the selection.

The results of the two-dimensional analysis of BEC in charged pion-pairs indicate that the longitudinal size of the pion emission region in $e^+e^- \rightarrow Z \rightarrow q\bar{q}$ events is larger than the transverse one. In Table 7 the values for the correlation radii obtained from ALEPH data for events with $T > 0.95$ are given, together with the values published

Table 6. The one-dimensional analysis results given by the LEP experiments. Only statistical errors are shown

	reference sample	λ	R (fm)
present study	mixed	0.36 ± 0.01	0.53 ± 0.01
	unlike-sign	0.44 ± 0.01	0.78 ± 0.01
ALEPH old	mixed	0.30 ± 0.11	0.51 ± 0.16
	unlike-sign	0.48 ± 0.03	0.81 ± 0.04
DELPHI	mixed	0.24 ± 0.02	0.47 ± 0.03
	unlike-sign	0.31 ± 0.02	0.83 ± 0.03
L3	mixed	0.29 ± 0.01	0.46 ± 0.01
OPAL	unlike-sign	0.87 ± 0.03	0.93 ± 0.02

Table 7. The two-dimensional analysis results given by the LEP experiments. Only statistical errors are shown

	reference sample	R_{T} (fm)	R_{L} (fm)	$R_{\mathrm{T}}/R_{\mathrm{L}}$
ALEPH	mixed	0.47 ± 0.01	0.77 ± 0.01	0.61 ± 0.01
	unlike-sign	0.79 ± 0.01	0.87 ± 0.02	0.91 ± 0.02
DELPHI	mixed	0.53 ± 0.02	0.85 ± 0.02	0.62 ± 0.02
L3	mixed	0.59 ± 0.01	0.74 ± 0.02	0.80 ± 0.02
OPAL	unlike-sign	0.81 ± 0.01	0.99 ± 0.01	0.82 ± 0.04

by DELPHI [13], L3 [14] and OPAL [15]. The L3 and OPAL collaborations have both published the results of a three-dimensional analysis, the corresponding values for R_{T} in Table 7 refer to the component perpendicular to the momentum sum.

The correlation radii R_{T} and R_{L} and the ratio $R_{\mathrm{T}}/R_{\mathrm{L}}$ were studied as a function of the two-jet purity by varying the thrust-cut, T_{cut}, between 0.90 and 0.97. The correlation radii as a function of T_{cut} behave differently when using the mixed and the unlike-sign reference sample. Using the mixed reference sample, R_{T} decreases with two-jet purity, while R_{L} is constant within 4%. Using instead the unlike-sign reference sample, the correlation radius R_{T} is independent of T_{cut}, while R_{L} stays constant within 6%. The influence of the quark-flavour composition on the results was studied, showing that the coherence strength factor λ increases with uds-purity, while the correlation radii R, R_{T} and R_{L} are not affected.

The outcome of this analysis shows that the choice of reference sample and the two-jet selection criterion used for the analysis have to be taken into account, in order to give an adequate interpretation of the obtained parameter values and to ensure a good comparison with results from other experiments.

References

1. G. Goldhaber et al., Pion-pion correlations in antiproton annihilation events, Phys. Rev. Lett. **3**, 181 (1959)
2. B. Lörstad, Boson Interferometry – A Review of high-energy data and its interpretation, Int. J. Mod. Phys. A **4**, 2861 (1989); D.H. Boal, C.K. Gelbke, B.K. Jennings, Intensity interferometry in subatomic physics, Rev. Mod. Phys. **62**, 553 (1990); G. Baym, The physics of Hanbury Brown-Twiss intensity interferometry: from stars to nuclear collisions, Acta Phys. Polon. B **29**, 1839 (1998); G. Alexander, Bose-Einstein and Fermi-Dirac interferometry in particle physics, Rep. Prog. Phys. **66**, 481 (2003)
3. Mark II Coll., D. Schlatter et al., Measurement of energy correlations in $e^+e^- \rightarrow$ hadrons, Phys. Rev. Lett. **49**, 521 (1982)
4. CLEO Coll., P. Avery et al., Bose-Einstein correlations in e^+e^- annihilation in the Υ region, Phys. Rev. D **32**, 2294 (1985)
5. TASSO Coll., M. Althoff et al., Bose-Einstein correlations observed in e^+e^- annihilation at a center-of-mass energy of 34 GeV, Z. Phys C **30**, 355 (1986)
6. TPC Coll., H. Aihara et al., Study of Bose-Einstein correlations in e^+e^- annihilation at 29 GeV, Phys. Rev. D **31**, 996 (1985)
7. ALEPH Coll., D. Decamp et al., A study of Bose-Einstein correlations in e^+e^- annihilation at 91 GeV, Z. Phys. C **54**, 75 (1992)
8. DELPHI Coll., P. Abreu et al., Bose-Einstein correlations in the hadronic decays of the Z, Phys. Lett. B **286**, 201 (1992)
9. L3 Coll., P. Achard et al., Bose-Einstein correlations of neutral and charged pions in hadronic Z decays, Phys. Lett. B **524**, 55 (2002)
10. OPAL Coll., P.D. Acton et. al., A study of Bose-Einstein Correlations in e^+e^- annihilations at LEP, Phys. Lett. B **267**, 143 (1991)
11. B. Andersson, G. Gustafson, G. Ingelman, T. Sjöstrand, Parton fragmentation and string dynamics, Phys. Rep. **97**, 31 (1983)
12. B. Andersson, M. Ringnér, Transverse and longitudinal Bose-Einstein correlations, Phys. Lett. B **421**, 283 (1998); Bose-Einstein correlations in the Lund model, Nucl. Phys. B **513**, 627 (1998)
13. DELPHI Coll., P. Abreu et al., Two-dimensional analysis of the Bose-Einstein correlations in e^+e^- annihilation at the Z peak, Phys. Lett. B **471**, 460 (2000)
14. L3 Coll., M. Acciarri et al., Measurement of an elongation of the pion source in Z decays, Phys. Lett. B **458**, 517 (1999)
15. OPAL Coll., G. Abbiendi et al., Transverse and longitudinal Bose-Einstein correlations in hadronic Z^0 decays, Eur. Phys. J. C **16**, 423 (2000)
16. T. Sjöstrand et al., High-energy physics event generation with Pythia 6.1 , Comp. Phys. Comm. **135**, 238 (2001)
17. G. Goldhaber, S. Goldhaber, W.Y. Lee, A. Pais, Influence of Bose-Einstein statistics on the antiproton proton annihilation process, Phys. Rev. **120**, 300 (1960); M. Deutschmann et al., A study of second-order interference for pions produced in various hadronic interactions, Nucl. Phys. B **204**, 333 (1982)
18. M.G. Bowler, Bose-Einstein symmetrization, coherence and chaos, with particular application to e^+e^- annihilation, Z. Phys. C **29** (1985)
19. ALEPH Coll., D. Decamp et al.,ALEPH: A detector for Electron-positron annihilations at LEP, Nucl. Instrum. Methods A **294**, 121 (1990)

20. ALEPH Coll., D. Buskulic et al., Performance of the ALEPH detector at LEP, Nucl. Instrum. Methods A **360**, 481 (1995)
21. ALEPH Coll., R. Barate et al., Studies of quantum chromodynamics with the ALEPH detector, Phys. Rep. **294**, 1 (1996)
22. ALEPH Coll., R. Barate et al., A precise measurement of $\Gamma_{Z \to b\bar{b}}/\Gamma_{Z \to \mathrm{hadrons}}$, Phys. Lett. B **313**, 535 (1993)
23. S. Haywood, Where are we going with Bose-Einstein – A mini review, Rutherford Lab. Report RAL-94-074 (1995)
24. K. Fialkowski, R. Wit, A note on Monte Carlo imitation of Bose-Einstein interference effects, Z. Phys. C **74**, 145 (1997)
25. L. Lönnblad, T. Sjöstrand, Modelling Bose-Einstein correlations at LEP 2, Eur. Phys. J. C **2**, 165 (1998)
26. R. Muresan, O. Smirnova, B. Lörstad, Appearance of an artificial length scale in JETSET Bose-Einstein simulation, Eur. Phys. J. C **6**, 629 (1999)
27. O. Smirnova, B. Lörstad, R. Muresan, Tests of the JETSET Bose-Einstein correlation model in the $e^{+}e^{-}$ annihilation process, arXiv:hep-ex/9808032
28. S. Catani et al., New clustering algorithm for multi-jet cross-sections in $e^{+}e^{-}$ annihilation, Phys. Lett. B **269**, 432 (1991)